Micro-EDM milling as a potential technique for fabrication of artificial defects on bearing raceways for accelerated testing

WCMNM 2020

Long Ye[1,2] , Krishna Kumar Saxena [1,2] , Jun Qian[1,2] , Dominiek Reynaerts[1,2]

[1]*Micro -& Precision Engineering Group, Department of Mechanical Engineering, KU Leuven, Belgium*
[2] *Members Flanders Make (https://www.flandersmake.be/en), Leuven, Belgium*

Abstract

Fabrication of artificial defects on bearing raceways helps in mimicking the incipient faults during real application or for directly validating the diagnostic technology depending on their shapes and sizes. This is particularly useful when run-to-failure experiments are time-consuming and even difficult in some cases. However, there is limited systematic research found on design and fabrication of the artificial defects on bearing raceways. In this work, micro-EDM is put forward as a potential technique for fabrication of artificial defects. In this paper a methodology is developed, not only to achieve full control of the dimension and distribution of defects on a bearing element, but also to perform efficient characterization of the defect surface qualitatively and quantitatively. A linear regression model based on analysis of variance (ANOVA) is presented to optimally select process parameters. The verification experiments show that this mathematical model obtains a good fit for about 80% of the observed data. Through a combination of stereo microscope and confocal microscope, the morphology and topography of the artificial defects is measured and compared. To conclude, it is shown that for optimum process parameters, micro-EDM has a better capability to fabricate a desirable feature shape which act as bearing defects.

Keywords: Artificial bearing defects, micro-EDM, bearings, tribology.

1. Introduction

Rolling/ball element bearings are indispensable components which are widely used for rotating machines. On the other hand, they are susceptible to failure due to deteriorated operating conditions and reduced fatigue strength, leading to unexpected machine downtime and eventually environmental pollution and economic loss. Therefore, the techniques involved with bearing condition monitoring are employed based on either vibration signals [1] or acoustic signals (AE) [2], which are collected through a run-to-failure or degradation tests. However, these tests are time-consuming and thus are not applicable to the verification of detection technology, for instance the machine learning driven method, which requires a huge training set. For this reason, artificial defects are induced in the form of indentation, line spalling or square wear to shorten the incipient period of growing bearing faults.

Although artificial defects are extensively used in bearing fault diagnostics and prognostics, their fabrication technique as well as shape and dimension have not been standardized. To investigate the AE technique for identifying bearing defects, Al-Ghamd et al. [3] introduced point defects, line defects and big rough defects in dimensions of 0.85×0.85 mm, 5.6×1.2 mm and 17.5×9.0 mm, respectively, on an outer raceway for simulating varying severity. The line defect was further tested with seven sizes to authenticate observations related to AE. Similarly, Hemmati [4] studied two fault geometries, i.e. a radial notch and a narrow line, on different bearing locations to mimic real defects. In their work, the width of a line defect was 1 to 2 mm while the diameter of a radial notch was 1 to 2 mm. To demonstrate the application of a fiber-optic sensor in estimating fault size, Alian et al. [5] seeded the artificial line-spalling defects in ten different widths ranging from 0.39 mm to 4 mm on both outer and inner races. The fault location was distributed along 12 angular orientations to differentiate the load.

Various alternative processing techniques for producing bearing defects have been reported in prior state-of-the-art. Al-Ghamd et al. [3] and Hemmati [4] engraved the artificial defects while Alian H et al. [5] produced the defects with EDM. Additionally, laser machining has been also reported to manufacture features mimicking bearing defects [6]. In view of the difficulty in maintaining the geometric consistency when applying engraving and laser machining, EDM seems to be more promising in producing artificial bearing defects practically and economically. Its non-contact machining traits enable machining on bearing races independent of hardness. As a downscaled process-variant of EDM, micro-EDM has capability to manufacture miniaturized components with features in submillimeter scale and with machining accuracy of 2-3 µm. This paper reports on the application of micro-EDM milling to artificially introduce pitting, line-spalling and notch bearing defects. This saves considerable time spent in run-to-failure bearing diagnostics. Since the machining efficiency is subjected to process stability, a design of experiments (DoE) was conducted to select optimal process parameters. Confocal measurements of the profile and topography of the machined defects are also presented to demonstrate successful machining of artificial defects on bearing races.

2. Experimental set-up

In this research, fabrication of artificial defects was carried out using micro-EDM on an SKF® spherical roller thrust bearing and an SNFA® ball bearing made of SKF Xbite heat treated steel and SAE 52100 chrome steel respectively. The experimental campaign was conducted on a standard Sarix® SX-100-HPM machine, which is shown in Fig. 1. In the right part of the machine, a wire electrical discharge

grinding (WEDG) device is attached to fabricate an electrode down to tens of microns in diameter. The wire between two plates is used for roughing after which the wire transferred around the blocks is used for finishing. A single station vise along the Y-axis is fixed by two step set-up clamps, which are bolted into the tooling plate. The ball bearing element fixed on the Y-axis can be tuned to any angle relative to X-axis to avoid collision with the milling spindle. The yellow tube is to provide external flushing during the process.

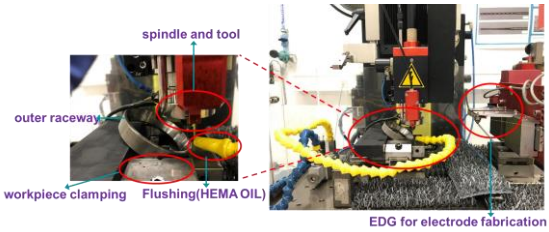

Fig. 1. Micro-EDM milling set-up for artificial defects machining.

HEDMA oil is used as dielectric in this experiment. In the top of the picture, a spindle, whose rotation speed could be up to 600 RPM, is attached to the frame through a System 3R chuck. The tool length is maintained constant through automatic electrode feeding where the wear of tool length is measured by electrical touch on the workpiece surface. In order to have minimal tool wear, a tungsten carbide rod of diameter 0.5 mm is used as milling electrode.

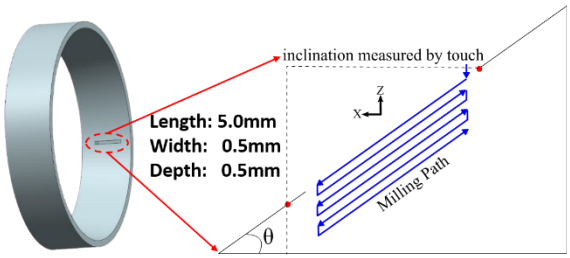

Fig. 2. Tool path of milling spalling on thrust bearing outer raceway. The two red points are touch points to measure the inclination angle θ.

Next, the milling strategy (tool path), has been determined. For milling on the outer raceway of the thrust bearing, the tool path was programmed back-and-forth along the inclined surface, whose slope was measured by an electric touch on two points as shown in Fig. 2. For milling on the inner raceway of the ball bearing, the tool path was kept concentric following the outside contour of the defects to be machined. The machining time for pitting and spalling defects is around 30 seconds and 2 minutes respectively.

3. Parameter optimization with statistical analysis

The EDM performance indices, e.g. material removal rate (MRR) and tool wear rate (TWR), mainly depend on the process stability, which is subject to not only the servo parameters but also to the electrical parameters. Therefore, a statistical model to quantify the inter-relationship between these factors and the final performance is necessary. In this research, a linear regression model based on analysis of variance (ANOVA) has been applied.

The pulse frequency, gap current, regulation gain and servo voltage were selected as main parameters and their levels are shown in Table 1. As aforementioned, MRR and TWR were selected as main performance indicators related to the economics of micro-EDM process for fabrication of bearing defects. MRR and TWR in this specific configuration were evaluated from Eqs. 1.

$$MRR[mm^3/min] = \pi r^2 \times l\,/t$$
$$TWR[mm^3/min] = \pi r^2 \times \Delta l\,/t \quad (1)$$

where r denotes the radius of electrode, $l, \Delta l$ denote the drilling depth and longitudinal tool wear respectively and t is the machining time. In order to perform the experiments within reasonable time, a two-level full factorial design was used by means of three repeated runs for axial points and seven runs for central points. The run order was then randomized in order to balance uncontrollable effects.

Table 1: Machining parameters with their levels.

Factors	Abbreviation/ Notation	Levels	
		Low(-)	High(+)
pulse frequency/s^{-1}	*f / (A)*	60	120
current	*I / (B)*	90	140
[1]regulation gain	*Kgain / (C)*	10	100
[2]servo voltage/V	*Ve / (D)*	40	70

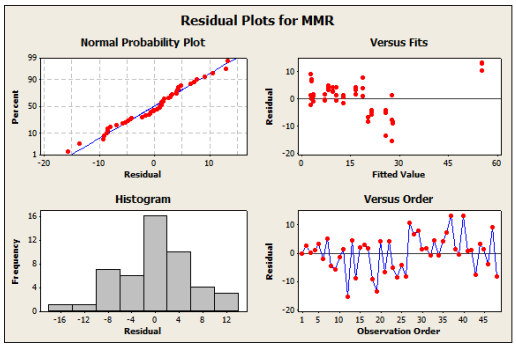

Fig. 3. Residual plots (four in one graph) for MRR as a response.

Figure 3 depicts the probability distribution of experimental data and can be approximated as a normal probability distribution for subsequent ANOVA analysis. And this normal distribution is further examined through histograms in the third plot, where a Gaussian curve could be found for fitting the values. The fourth plot of residuals versus order shows a random tendency guaranteeing uncorrelated errors for MRR and TWR. As a whole, this graph ensures the linear regression assumption that the error terms are independent and normally distributed with equal variance.

1 It is worth mentioning that the regulation gain is a representative of servo control reaction. The higher the regulation gain, the more quickly the system response to variations but this leads to more unstable behaviour of the system.

2 The servo voltage in micro-EDM refers to the target gap voltage over a certain period. It is a typical signature to reflect the gap condition. Generally, the higher the servo voltage, the bigger the gap and thus the more aggressiveness a EDM process exerts.

The P-value calculated based on F-statistic, which is shown in Table 3, is able to describe how significant each effect term behaves in the regression model. When it is lower than the significance level, which is 0.05 in this paper, the null hypothesis is rejected meaning the corresponding term is effective. It is thus concluded that two-way interactions *A*D* are discarded for MRR, whereas the main term *C* along with two-way interactions *A*C* and *A*D* are discarded for TWR. Based on the selected terms, the R^2 statistics [7] calculated from the ANOVA table are 81.90% and 82.76% respectively for MRR and TWR, which indicates that approximately 80% of the observed variation could be explained by main effects and two-way interactions.

Table 2: ANOVA analysis[a]

Effects	MRR/ (mm^3/min)		TWR/ (mm^3/min)	
	F	P	F	P
A	42.66	0.00	119.39	0.00
B	19.53	0.00	17.98	0.00
C	6.34	0.00	1.21	0.28
D	26.63	0.02	10.18	0.00
A*B	26.86	0.00	4.46	0.04
A*C	4.90	0.00	0.30	0.59
A*D	1.23	0.27	0.23	0.64
B*C	17.83	0.00	11.66	0.00
B*D	17.54	0.00	9.44	0.00
C*D	30.91	0.00	28.54	0.00

[a]A denotes frequency, B denotes current, C denotes Kgain, D denotes Ve. The terms corresponding to higher than two-way interactions are omitted.

Based on the ANOVA analysis, the linear regression models, in which MRR and TWR are taken as outputs, are derived as follows:

$$\widehat{MRR} = 16.81 - 6.14 \times A + 4.15 \times B - 2.37 \times C + 4.85 \times D - 4.87 \times (A * B) + 2.08 \times (A * C) - 3.97 \times (B * C) + 3.94 \times (B * D) - 5.22 \times (C * D) \quad (2)$$

$$\widehat{TWR} = 12.07 - 6.26 \times A + 2.43 \times B + 1.83 \times D - 1.21 \times (A * B) - 1.96 \times (B * C) + 1.76 \times (B * D) - 3.06 \times (C * D) \quad (3)$$

where the coefficients fitted in the models are obtained from estimated effects. By specifying targeted MRR and TWR (0.15 mm^3/min and 0.04 mm^3/min), the optimal parameters are accordingly determined using equation (2) and (3).

4. Characterization of artificial bearing defects

The bearing defect usually grows from a surface imperfection in the incipient phase to a damaged area in the failed phase. A typical example is presented in Fig.4 where five stages of defect on the inner ring are generated during an accelerated test. It is visually obvious that the defect expands not only along the raceway but also inwards radially. This might be the result of uneven stress on the defected part when running. For pilot research, Vicker indentation was applied to create a defect on bearing element, however it was difficult to control feature shape, distribution and accuracy due to local deformation caused by mechanical indentation. Moreover, Vicker hardness testers are not CNC machines and therefore automation of process is difficult and also limited as compared to the manufacturing capabilities of a micro-EDM machine.

Once the artificial defects were machined, they were measured first with a stereo microscope ZEISS© for fast inspection and then with a confocal microscope Sensofar Neox© for quantitative characterization. The machined defects on the bearing interacting surfaces of each element are shown in Fig.5. The pittings on the outer raceway as shown in Fig. 5(a) are uniformly distributed along the shaft axis. Their diameters in one row are around 550 ± 5 µm. This machined feature is comparatively small in order to mimic an incipient defect thereby enabling the observation of its evolving under different operating conditions. The spalling with width 500 µm and depth 2000 µm shown in Fig. 5(b) was machined radially onto the inner raceway. This

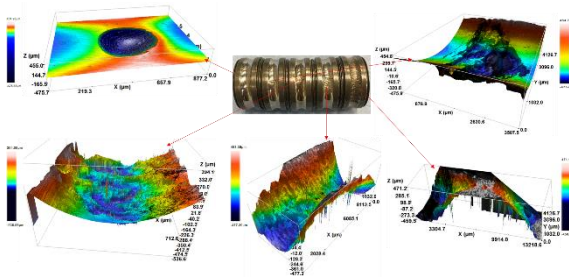

Fig. 4. Confocal characterization of running bearing defects starting from an indentation. The figures from left to right and top to bottom are correspondingly the 3D topography of defects in different severities. Measurement by Sensofar S Neox, with objective 20x, restoration applied

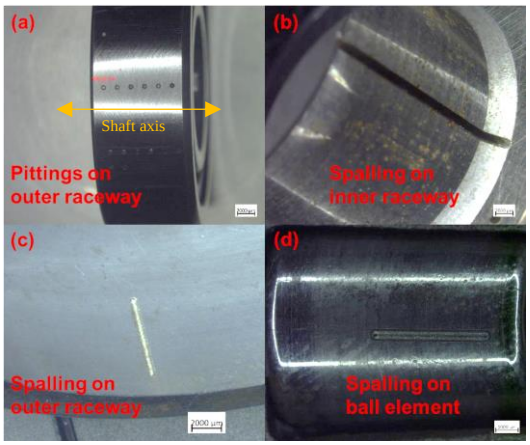

Fig. 5. Geometrical measurement of artificial defects by stereo microscope (a) pittings on outer raceway (b) spalling on inner raceway (c) spalling on outer raceway (d) spalling on ball element. Measurement by a Zeiss® SteREO Discovery V20 microscope

artificial feature is relatively large in order to mimic a running fault in the grown stage thereby enabling the validation of newly-developed detection technologies.

The spalling shown in Fig. 5(c) corresponds to the designed feature in Fig. 2. The same feature was also copied to the ball element which has a direct contact with the outer raceway. Being able to mimic the main features of surface fatigue that leads to bearing failure under proper lubrication and operating conditions, this bearing defect is specially designed for the test rig which is later used for an estimation of the bearing

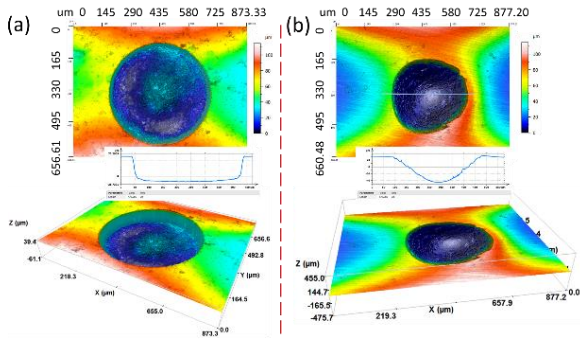

Fig. 6. 2D/3D topography and profile of artificial defects (a) pitting produced by micro-EDM (b) indentation produced by Vickers hardness machine. Measurement by Sensofar S Neox,

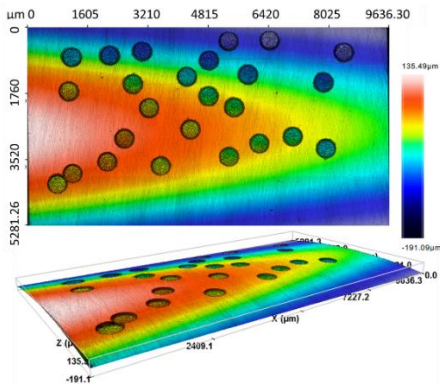

Fig. 7. Random pittings generated by micro-EDM on a bearing outer ring. Measurement by Sensofar S Neox, with objective 20x, restoration applied, no filtration applied

remaining useful life.

Fig. 6 shows the quantitative comparison of the topologies of the micro-EDMed pitting and indentation. Since the diamond indenter used in the Vickers hardness tester is of conical shape, the profile of indentation appears like a round V shape. Although the depth of the pitting is the same as that of the indentation, its profile looks like a U shape because of inevitable corner wear showing up on the cylindrical electrode when machining. Furthermore, by changing the process parameters introduced in Section 3, the bottom corner angle and outline can be tuned with respect to the topography of a running defect. In addition, it can be seen that there is obvious build-up around the indent edge due to local material deformation during indenting process. Whereas the pitting edge seems smooth and consistent after an optimized micro-EDM process, alleviating the topological effects that cannot be quantitively evaluated upon acceleration test results.

As shown in Fig. 7, the randomly generated pittings were fabricated on a specific area of the bearing outer surface. This distribution mimics real bearing defects due to the fact that some pittings are much more likely to appear in a group when the lubrication is highly contaminated by exotic particles. By using a post-program before drilling, a set of pittings with a pre-defined hole area ratio, e.g. 15% in this paper, are irregularly generated. The generated pittings are then re-located in a user-defined reference and their coordinate information is sent to an operating program in the EDM machine for automatic drilling. In Fig. 7, all the pittings are distributed with the same diameter and depth, i.e. 500 µm and 70 µm respectively. However, the pittings can also be produced with varying topologies when using WEDG for fabricating the tool electrodes. Since, there is a restriction applied on the pitch between the holes, all pittings are observed separately. By taking into account the randomness and shape (diameter, depth, surface quality) of the distributed pittings, the capabilities of micro-EDM in generating the artificial bearing defects to be more comparable to natural defects have been demonstrated and assessed.

5. Conclusions

This work demonstrated and assessed the potential of micro-EDM technology in fabrication of artificial defects on bearing races, thereby minimizing time spent in run-to-failure bearing diagnostics. A holistic approach was adopted using a combination of design of experiments, ANOVA analysis, confocal measurements to evaluate the machined defects. The machined defects in the form of pitting and spalling have been characterized as running defects in different levels of severity. Randomly distributed pittings have also been mimicked to be comparable to their real cases in a highly contaminated environment. Finally, the difference of the artificially induced pitting and indentation in topography has been identified by confocal measurements. To conclude, it is shown that for optimum process parameters, micro-EDM has a better capability (MRR 0.15 mm^3/min and TWR 0.04 mm^3/min) to fabricate a desirable feature shape which act as bearing defects.

Future work is planned to characterize the sub-surface cracks introduced by the artificial bearing defects and investigate what effects they will have on a running test.

Acknowledgements

This work is partially sponsored by Flanders Make covenant dotation for exploratory research.

References

[1] Ali JB et al. “Application of empirical mode decomposition and artificial neural network for automatic bearing fault diagnosis based on vibration signals,” Applied Acoustics., 2015, 89:16-27.

[2] Tandon N et al. “A review of vibration and acoustic measurement methods for the detection of defects in rolling element bearings,” Tribology international., 1999, 32(8):469-80.

[3] Al-Ghamd AM et al. “A comparative experimental study on the use of acoustic emission and vibration analysis for bearing defect identification and estimation of defect size,” Mechanical systems and signal processing., 2006, 20(7):1537-71.

[4] Hemmati F. “Rolling element bearing condition monitoring using acoustic emission technique and advanced signal processing,” 2010.

[5] Alian H et al. “Bearing fault detection and fault size estimation using fiber-optic sensors,” Mechanical Systems and Signal Processing., 2019, 120:392-407.

[6] Pandya D et al., “Fault diagnosis of rolling element bearing by using multinomial logistic regression and wavelet packet transform ,” Soft Computing: 2014, 18(2):255-66.

[7] Montgomery DC et al., Engineering statistics. John Wiley & Sons: 2009, 311.